
Multiple Futures Prediction

Yichuan Charlie Tang
Apple Inc.
yichuan_tang@apple.com

Ruslan Salakhutdinov
Apple Inc.
rsalakhutdinov@apple.com

Abstract

Temporal prediction is critical for making intelligent and robust decisions in complex dynamic environments. Motion prediction needs to model the inherently uncertain future which often contains multiple potential outcomes, due to multi-agent interactions and the latent goals of others. Towards these goals, we introduce a probabilistic framework that efficiently learns latent variables to jointly model the multi-step future motions of agents in a scene. Our framework is data-driven and learns semantically meaningful latent variables to represent the multimodal future, without requiring explicit labels. Using a dynamic attention-based state encoder, we learn to encode the past as well as the *future* interactions among agents, efficiently scaling to any number of agents. Finally, our model can be used for planning via computing a conditional probability density over the trajectories of other agents given a hypothetical rollout of the ‘self’ agent. We demonstrate our algorithms by predicting vehicle trajectories of both simulated and real data, demonstrating the *state-of-the-art* results on several vehicle trajectory datasets.

1 Introduction

The ability to make good predictions lies at the heart of robust and safe decision making. It is especially critical to be able to predict the future motions of all relevant agents in complex and dynamic environments. For example, in the autonomous driving domain, motion prediction is central both to the ability to make high level decisions, such as when to perform maneuvers, as well as to low level path planning optimizations [34, 28].

Motion prediction is a challenging problem due to the various needs of a good predictive model. The varying objectives, goals, and behavioral characteristics of different agents can lead to multiple possible futures or modes. Agents’ states do not evolve independently from one another, but rather they interact with each other. As an illustration, we provide some examples in Fig. 1. In Fig. 1(a), there are a few different possible futures for the blue vehicle approaching an intersection. It can either turn left, go straight, or turn right, forming different modes in trajectory space. In Fig. 1(b), interactions between the two vehicles during a merge scenario show that their trajectories influence each other, depending on who yields to whom. Besides multimodal interactions, prediction needs to scale efficiently with an arbitrary number of agents in a scene and take into account auxiliary and contextual information, such as map and road information. Additionally, the ability to measure uncertainty by computing probability over likely future trajectories of all agents in closed-form (as opposed to Monte Carlo sampling) is of practical importance.

Despite a large body of work in temporal motion predictions [24, 7, 13, 26, 16, 2, 30, 8, 39], existing state-of-the-art methods often only capture a subset of the aforementioned features. For example, algorithms are either deterministic, not multimodal, or do not fully capture both past and future interactions. Multimodal techniques often require the explicit labeling of modes prior to training. Models which perform joint prediction often assume the number of agents present to be fixed [36, 31].

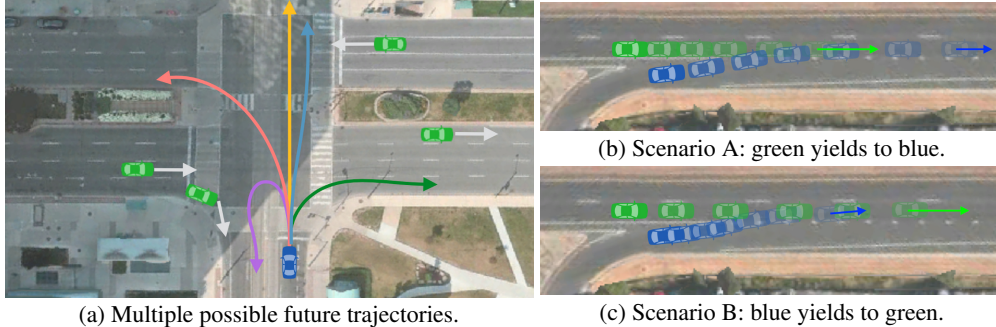


Figure 1: Examples illustrating the need for multimodal interactive predictions. (a): There are a few possible modes for the blue vehicle. (b and c): Time-lapsed visualization of how interactions between agents influences each other’s trajectories.

We tackle these challenges by proposing a unifying framework that captures all of the desirable features mentioned earlier. Our framework, which we call Multiple Futures Predictor (MFP), is a sequential probabilistic latent variable generative model that learns directly from multi-agent trajectory data. Training maximizes a variational lower bound on the log-likelihood of the data. MFP learns to model multimodal interactive futures *jointly* for all agents, while using a novel factorization technique to remain scalable to arbitrary number of agents. After training, MFP can compute both (un)conditional trajectory probabilities in closed form, not requiring any Monte Carlo sampling.

MFP builds on the Seq2seq [32], encoder-decoder framework by introducing latent variables and using a set of parallel RNNs (with shared weights) to represent the set of agents in a scene. Each RNN takes on the point-of-view of its agent and aggregates historical information for sequential temporal prediction for that agent. Discrete latent variables, one per RNN, automatically learn semantically meaningful modes to capture multimodality without explicit labeling. MFP can be further efficiently and jointly trained end-to-end for all agents in the scene. To summarize, we make the following contributions: First, semantically meaningful latent variables are automatically learned from trajectory data *without* labels. This addresses the **multimodality** problem. Second, interactive and parallel step-wise rollouts are preformed for all agents in the scene. This addresses the modeling of **interactions** between actors during future prediction, see Sec. 3.1. We further propose a dynamic attentional encoding which captures both the relationships between agents and the scene context, see Sec. 3.1. Finally, MFP is capable of performing hypothetical inference: evaluating the conditional probability of agents’ trajectories conditioning on fixing one or more agent’s trajectory, see Sec. 3.2.

2 Related Work

The problem of predicting future motion for dynamic agents has been well studied in the literature. The bulk of classical methods focus on using physics based dynamic or kinematic models [38, 21, 25]. These approaches include Kalman filters and maneuver based methods, which compute the future motion of agents by propagating their current state forward in time. While these methods perform well for short time horizons, longer horizons suffer due to the lack of interaction and context modeling.

The success of machine learning and deep learning ushered in a variety of data-driven recurrent neural network (RNN) based methods [24, 7, 13, 26, 16, 2]. These models often combine RNN variants, such as LSTMs or GRUs, with encoder-decoder architectures such as conditional variational autoencoders (CVAEs). These methods eschew physic based dynamic models in favor of learning generic sequential predictors (e.g. RNNs) directly from data. Converting raw input data to input features can also be learned, often by encoding rasterized inputs using CNNs [7, 13].

Methods that can learn multiple future modes have been proposed in [16, 24, 13]. However, [16] explicitly labels six maneuvers/modes and learn to separately classify these modes. [24, 13] do not require mode labeling but they also do not train in an end-to-end fashion by maximizing the data log-likelihood of the model. Most of the methods in literature encode the *past* interactions of agents in a scene, however prediction is often an independent rollout of a decoder RNN, independent of other future predicted trajectories [16, 29]. Encoding of spatial relationships is often done by placing other agents in a fixed and spatially discretized grid [16, 24].

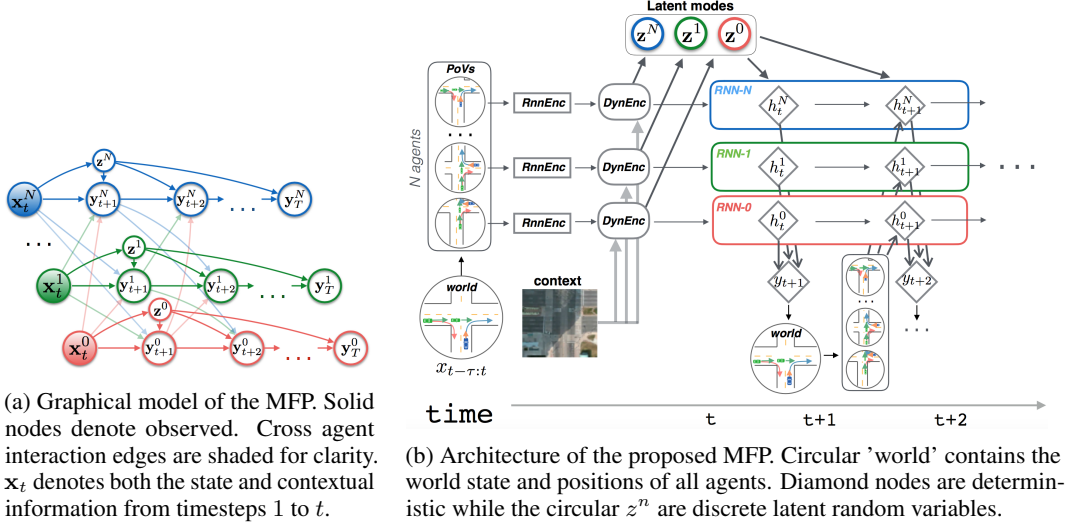


Figure 2: Graphical model and computation graph of the MFP. See text for details. Best viewed in color.

In contrast, MFP proposes a unifying framework which exhibits the aforementioned features. To summarize, we present a feature comparison of MFP with some of the recent methods in the supplementary materials.

3 Multiple Futures Prediction

We tackle motion prediction by formulating a probabilistic framework of continuous space but discrete time system with a finite (but variable) number of N interacting agents. We represent the joint state of all N agents at time t as $\mathbf{X}_t \in \mathbb{R}^{N \times d} \doteq \{\mathbf{x}_t^1, \mathbf{x}_t^2, \dots, \mathbf{x}_t^N\}$, where d is the dimensionality of each state¹, and $\mathbf{x}_t^n \in \mathbb{R}^d$ is the state n -th agent at time t . With a slight abuse of notation, we use superscripted $\mathbf{X}^n \doteq \{\mathbf{x}_{t-\tau}^n, \mathbf{x}_{t-\tau+1}^n, \dots, \mathbf{x}_t^n\}$ to denote the past states of the n -th agent and $\mathbf{X} \doteq \mathbf{X}_{t-\tau:t}^{1:N}$ to denote the joint agent states from time $t - \tau$ to t , where τ is the past history steps. The future state at time δ of all agents is denoted by $\mathbf{Y}_\delta \doteq \{\mathbf{y}_\delta^1, \mathbf{y}_\delta^2, \dots, \mathbf{y}_\delta^N\}$ and the future trajectory of agent n , from time t to time T , is denoted by $\mathbf{Y}^n \doteq \{\mathbf{y}_t^n, \mathbf{y}_{t+1}^n, \dots, \mathbf{y}_T^n\}$. $\mathbf{Y} \doteq \mathbf{Y}_{t:t+T}^{1:N}$ denotes the joint state of all agents for the future timesteps. Contextual scene information, e.g. a rasterized image $\mathbb{R}^{h \times w \times 3}$ of the map, could be useful by providing important cues. We use \mathcal{I}_t to represent any contextual information at time t .

The goal of motion prediction is then to accurately model $p(\mathbf{Y}|\mathbf{X}, \mathcal{I}_t)$. As in most sequential modelling tasks, it is both inefficient and intractable to model $p(\mathbf{Y}|\mathbf{X}, \mathcal{I}_t)$ jointly. RNNs are typically employed to sequentially model the distribution in a cascade form. However, there are two major challenges specific to our multi-agent prediction framework: (1) **Multimodality**: optimizing vanilla RNNs via backpropagation through time will lead to *mode-averaging* since the mapping from \mathbf{X} to \mathbf{Y} is not a *function*, but rather a one-to-many mapping. In other words, multimodality means that for a given \mathbf{X} , there could be multiple distinctive modes that results in significant probability distribution over different sequences of \mathbf{Y} . (2) **Variable-Agents**: the number of agents N is variable and *unknown*, and therefore we can not simply vectorize \mathbf{X}_t as the input to a standard RNN at time t .

For multimodality, we introduce a set of stochastic latent variables $z^n \sim \text{Multinoulli}(K)$, one per agent, where z^n can take on K discrete values. The intuition here is that z^n would learn to represent intentions (left/right/straight) and/or behavior modes (aggressive/conservative). Learning maximizes the marginalized distribution, where z is free to learn any latent behavior so long as it helps to improve the data log-likelihood. Each z is conditioned on X at the current time (before future prediction) and will influence the distribution over future states \mathbf{Y} . A key feature of the MFP is that z^n is only sampled once at time t , and must be consistent for the next T time steps. Compared to sampling z^n at every timestep, this leads to a tractability and more realistic intention/goal modeling,

¹We assume states are fully observable and are agents' (x, y) coordinates on the ground plane ($d=2$).

as we will discuss in more detail later. We now arrive at the following distribution:

$$\log p(\mathbf{Y}|\mathbf{X}, \mathcal{I}) = \log\left(\sum_Z p(\mathbf{Y}, Z|\mathbf{X}, \mathcal{I})\right) = \log\left(\sum_Z p(\mathbf{Y}|Z, \mathbf{X}, \mathcal{I})p(Z|\mathbf{X}, \mathcal{I})\right), \quad (1)$$

where Z denotes the joint latent variables of all agents. Naïvely optimizing for Eq. 1 is prohibitively expensive and not scalable as the number of agents and timesteps may become large. In addition, the max number of possible modes is exponential: $\mathcal{O}(K^N)$. We first make the model more tractable by factorizing across time, followed by factorization across agents. The joint future distribution \mathbf{Y} assumes the form of product of conditional distributions:

$$p(\mathbf{Y}|Z, \mathbf{X}, \mathcal{I}) = \prod_{\delta=t+1}^T p(\mathbf{Y}_\delta|\mathbf{Y}_{t:\delta-1}, Z, \mathbf{X}, \mathcal{I}), \quad (2)$$

$$p(\mathbf{Y}_\delta|\mathbf{Y}_{t:\delta-1}, Z, \mathbf{X}, \mathcal{I}) = \prod_{n=1}^N p(\mathbf{y}_\delta^n|\mathbf{Y}_{t:\delta-1}, z^n, \mathbf{X}, \mathcal{I}). \quad (3)$$

The second factorization is sensible as the factorial component is conditioning on the *joint* states of all agents in the immediate previous timestep, where the typical temporal delta is very short (e.g. 100ms). Also note that the future distribution of the n -th agent is explicitly dependent on its own mode z^n but *implicitly* dependent on the latent modes of other agents by re-encoding the other agents predicted states \mathbf{y}_δ^n (please see discussion later and also Sec. 3.1). Explicitly conditioning an agent’s own latent modes is both more scalable computationally as well as more realistic: agents in the real-world can only infer other agent’s latent goals/intentions via observing their states. Finally our overall objective from Eq. 1 can be written as:

$$\log\left(\sum_Z p(\mathbf{Y}|Z, \mathbf{X}, \mathcal{I})p(Z|\mathbf{X}, \mathcal{I})\right) = \log\left(\sum_Z \prod_{\delta=t+1}^T \prod_{n=1}^N p(\mathbf{y}_\delta^n|\mathbf{Y}_{t:\delta-1}, z^n, \mathbf{X}, \mathcal{I})p(z^n|\mathbf{X}, \mathcal{I})\right) \quad (4)$$

$$= \log\left(\sum_Z \prod_{n=1}^N p(z^n|\mathbf{X}, \mathcal{I}) \prod_{\delta=t+1}^T p(\mathbf{y}_\delta^n|\mathbf{Y}_{t:\delta-1}, z^n, \mathbf{X}, \mathcal{I})\right) \quad (5)$$

The graphical model of the MFP is illustrated in Fig. 2a. While we show only three agents for simplicity, MFP can easily scale to any number of agents. Nonlinear interactions among agents makes $p(\mathbf{y}_\delta^n|\mathbf{Y}_{t:\delta-1}, \mathbf{X}, \mathcal{I})$ complicated to model. The class of recurrent neural networks are powerful and flexible models that can efficiently capture and represent long-term dependences in sequential data. At a high level, RNNs introduce deterministic hidden units h_t at every timestep t , which act as features or embeddings that summarize all of the observations up until time t . At time step t , a RNN takes as its input the observation, x_t , and the previous hidden representation, h_{t-1} , and computes the update: $h_t = f_{rnn}(x_t, h_{t-1})$. The prediction y_t is computed from the decoding layer of the RNN $y_t = f_{dec}(h_t)$. f_{rnn} and f_{dec} are recursively applied at every timestep of the sequence.

Fig. 8 shows the computation graph of the MFP. A *point-of-view* (PoV) transformation $\varphi^n(\mathbf{X}_t)$ is first used to transform the past states to each agent’s own reference frame by translation and rotation such that $+x$ -axis aligns with agent’s heading. We then instantiate an encoding and a decoding RNN² per agent. Each encoding RNN is responsible for encoding the *past* observations $\mathbf{x}_{t-\tau:t}$ into a feature vector. Scene context is transformed via a convolutional neural network into its own feature. The features are combined via a *dynamic attention encoder*, detailed in Sec. 3.1, to provide inputs both to the latent variables as well as to the ensuing decoding RNNs. During predictive rollouts, the decoding RNN will predict its own agent’s state at every timestep. The predictions will be aggregated and subsequently transformed via $\varphi^n(\cdot)$, providing inputs to every agent/RNN for the next timestep. Latent variables Z provide extra inputs to the decoding RNNs to enable multimodality. Finally, the output \mathbf{y}_t^n consists of a 5 dim vector governing a Bivariate Normal distribution: $\mu_x, \mu_y, \sigma_x, \sigma_y$, and correlation coefficient ρ .

While we instantiate two RNNs per agent, these RNNs *share* the same parameters across agents, which means we can efficiently perform joint predictions by combining inputs in a minibatch, allowing us to scale to *arbitrary* number of agents. Making Z discrete and having only one set of latent variables influencing subsequent predictions is also a deliberate choice. We would like Z to model modes generated due to high level intentions such as left/right lane changes or conservative/aggressive modes of agent behavior. These latent behavior modes also tend to stay consistent over the time horizon which is typical of motion prediction (e.g. 5 seconds).

²We use GRUs [10]. LSTMs and GRUs perform similarly, but GRUs were slightly faster computationally.

Learning

Given a set of training trajectory data $\mathcal{D} = \{(\mathbf{X}^{(i)}, \mathbf{Y}^{(i)})\}_{i=1,2,\dots,|\mathcal{D}|}$, we optimize using the maximum likelihood estimation (MLE) to estimate the parameters $\theta^* = \operatorname{argmax}_{\theta} \mathcal{L}(\theta, \mathcal{D})$ that achieves the maximum marginal data log-likelihood:³

$$\mathcal{L}(\theta, \mathcal{D}) = \log p(\mathbf{Y}|\mathbf{X}; \theta) = \log \left(\sum_Z p(\mathbf{Y}, Z|\mathbf{X}; \theta) \right) = \sum_Z p(Z|\mathbf{Y}, \mathbf{X}; \theta) \log \frac{p(\mathbf{Y}, Z|\mathbf{X}; \theta)}{p(Z|\mathbf{Y}, \mathbf{X}; \theta)} \quad (6)$$

Optimizing for Eq. 6 directly is non-trivial as the posterior distribution is not only hard to compute, but also varies with θ . We can however decompose the log-likelihood into the sum of the *evidence lower bound* (ELBO) and the KL-divergence between the true posterior and an approximating posterior $q(Z)$ [27]:

$$\begin{aligned} \log p(\mathbf{Y}|\mathbf{X}; \theta) &= \sum_Z q(Z|\mathbf{Y}, \mathbf{X}) \log \frac{p(\mathbf{Y}, Z|\mathbf{X}; \theta)}{q(Z|\mathbf{Y}, \mathbf{X})} + D_{KL}(q||p) \\ &\geq \sum_Z q(Z|\mathbf{Y}, \mathbf{X}) \log p(\mathbf{Y}, Z|\mathbf{X}; \theta) + H(q), \end{aligned} \quad (7)$$

where Jensen’s inequality is used to arrive at the lower bound, H is the entropy function and $D_{KL}(q||p)$ is the KL-divergence between the true and approximating posterior. We learn by maximizing the variational lower bound on the data log-likelihood by first using the true posterior⁴ at the current θ' as the approximating posterior: $q(Z|\mathbf{Y}, \mathbf{X}) \doteq p(Z|\mathbf{Y}, \mathbf{X}; \theta')$. We can then fix the approximate posterior and optimize the model parameters for the following function:

$$\begin{aligned} Q(\theta, \theta') &= \sum_Z p(Z|\mathbf{Y}, \mathbf{X}; \theta') \log p(\mathbf{Y}, Z|\mathbf{X}; \theta) \\ &= \sum_Z p(Z|\mathbf{Y}, \mathbf{X}; \theta') \{ \log p(\mathbf{Y}|Z, \mathbf{X}; \theta_{rnn}) + \log p(Z|\mathbf{X}; \theta_Z) \}. \end{aligned} \quad (8)$$

where $\theta = \{\theta_{rnn}, \theta_Z\}$ denote the parameters of the RNNs and the parameters of the network layers for predicting Z . As our latent variables Z are discrete and have small cardinality (e.g. < 10), we can compute the posterior exactly for a given θ' . The RNN parameter gradients are computed from $\partial Q(\theta, \theta')/\partial \theta_{rnn}$ and the gradient for θ_Z is $\partial KL(p(Z|\mathbf{Y}, \mathbf{X}; \theta')||p(Z|\mathbf{X}; \theta_Z))/\partial \theta_Z$.

Our learning algorithm is a form of the EM algorithm [14], where for the M-step we optimize RNN parameters using stochastic gradient descent. By integrating out the latent variable Z , MFP learns *directly* from trajectory data, without requiring any annotations or weak supervision for latent modes. We provide a detailed training algorithm pseudocode in the supplementary materials.

Classmates-forcing

Teacher forcing is a standard technique (albeit biased) to accelerate RNN and sequence-to-sequence training by using ground truth values y_t as the input to step $t + 1$. Even with scheduled sampling [4], we found that over-fitting due to *exposure bias* could be an issue. Interestingly, an alternative is possible in the MFP: for agent n , the ground truth observations are used as inputs for all other agents $y_t^m : m \neq n$. However, for agent n itself, we still use its previous predicted state instead of the true observations x_t^n as its input. We provide empirical comparisons in Table 2.

Connections to other Stochastic RNNs

Various stochastic recurrent models in existing literature have been proposed: DRAW [20], STORN [3], VRNN [11], SRNN [18], Z-forcing [19], Graph-VRNN [31]. Beside the multi-agent modeling capability of the MFP, the key difference between these methods and MFP is that the other methods use continuous stochastic latent variables z_t at *every* timestep, sampled from a standard Normal prior. The training is performed via the pathwise derivatives, or the reparameterization trick. Having multiple continuous stochastic variables means that the posterior can not be computed in closed form and Monte Carlo (or lower-variance MCMC estimators⁵) must be used to estimate the ELBO. This makes it hard to efficiently compute the log-probability of an arbitrary imagined or hypothetical trajectory, which might be useful for planning and decision-making (See Sec. 3.2). In contrast, latent variables in MFP is discrete and can learn semantically meaningful modes (Sec. 4.1).

³We have omitted the dependence on context \mathcal{I} for clarity. The R.H.S. is derived from the common *log-derivative trick*.

⁴The ELBO is the tightest when the KL-divergence is zero and the q is the true posterior.

⁵Even with IWAE [6], 50 samples are needed to obtain a somewhat tight lower-bound, making it prohibitively expensive to compute good log-densities for these stochastic RNNs for online applications.

With K modes, it is possible to evaluate the exact log-likelihoods of trajectories in $\mathcal{O}(K)$, without resorting to sampling.

3.1 State Encodings

As shown in Fig. 8, the input to the RNNs at step t is first transformed via the *point-of-view* $\varphi(\mathbf{Y}_t)$ transformation, followed by *state encoding*, which aggregates the relative positions of other agents with respect to the n -th agent (*ego* agent, or the agent for which the RNN is predicting) and encodes the information into a feature vector. We denote the encoded feature $\mathbf{s}_t \leftarrow \phi_{enc}^n(\varphi(\mathbf{Y}_t))$. Here, we propose a dynamic attention-like mechanism where radial basis functions are used for matching and routing relevant agents from the input to the feature encoder, shown in Fig. 3.

Each agent uses a neural network to transform its state (positions, velocity, acceleration, and heading) into a key or descriptor, which is then matched via a radial basis function to a fixed number of ‘‘slots’’ with learned keys in the encoder network. The ego⁶ agent has a separate slot to send its own state. Slots are aggregated and further transformed by a two layer encoder network, encoding a state \mathbf{s}_t (e.g. 128 dim vector). The entire dynamic encoder can be learned in an end-to-end fashion. The key-matching is similar to dot-product attention [35], however, the use of radial basis functions allows us to learn spatially sensitive and meaningful keys to extract relevant agents. In addition, Softmax normalization in dot-product attention lacks the ability to differentiate between a *single* close-by agent vs. a far-away agent.

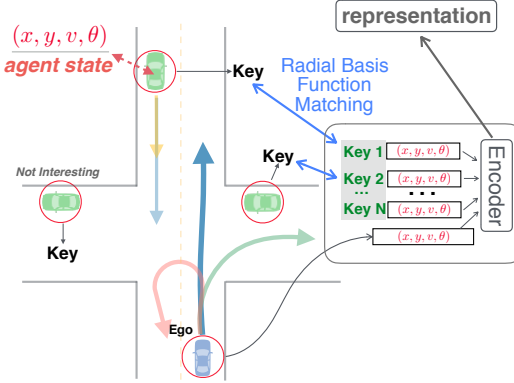


Figure 3: Diagram for dynamic attentional state encoding. MFP uses state encoding at every timestep to convert the state of surrounding agents into a feature vector for next-step prediction, see text for more details.

3.2 Hypothetical Rollouts

Planning and decision-making must rely on prediction for *what-ifs* [22]. It is important to predict how others might behave to different *hypothetical* ego actions (e.g. what if ego were to perform a more aggressive lane change?). Specifically, we are interested in the distribution when conditioning on any hypothetical future trajectory \mathbf{Y}^n of one (or more) agents:

$$p(\mathbf{Y}^{m:m \neq n} | \mathbf{Y}^n, \mathbf{X}) = \sum_{Z^{m:m \neq n}} \prod_{\delta=t+1}^T \prod_{m:m \neq n}^N p(\mathbf{y}_\delta^m | \mathbf{Y}_{t:\delta-1}, z^m, \mathbf{X}) p(z^m | \mathbf{X}), \quad (9)$$

This can be easily computed within MFP by fixing future states $\mathbf{y}_{t:T}^n$ of the conditioning agent on the R.H.S. of Eq. 9 while the states of other agents $\mathbf{y}_{t:T}^{m \neq n}$ are not changed. This is due to the fact that MFP performs interactive *future* rollouts in a synchronized manner for all agents, as the joint *predicted* states at t of all agents are used as inputs for predicting the states at $t + 1$. As a comparison, most of the other prediction algorithms perform independent rollouts, which makes it impossible to perform hypothetical rollouts as there is a lack of interactions during the future timesteps.

4 Experimental Results

We demonstrate the effectiveness of MFP in learning interactive multimodal predictions for the driving domain, where each agent is a vehicle. As a proof-of-concept, we first generate simulated trajectory data from the CARLA simulator [17], where we can specify the number of modes and script 2nd-order interactions. We demonstrate MFP can learn semantically meaningful latent modes to capture all of the modes of the data, all without using labeling of the latent modes. We then experiment on a widely known standard dataset of real vehicle trajectories, the NGSIM [12] dataset. We show that MFP achieves *state-of-the-art* results on modeling held-out test trajectories. In addition, we also benchmark MFP with previously published results on the more recent large scale Argoverse motion forecasting dataset [9]. We provide MFP architecture and learning details in the supplementary materials.

⁶We will use ego to refer to the main or ‘self’ agent for whom we are predicting.

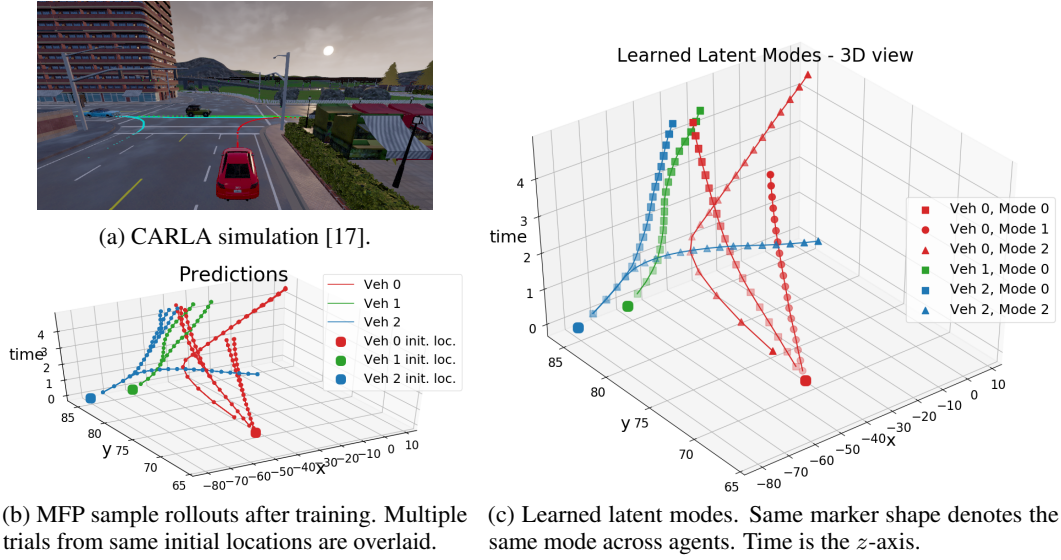


Figure 4: (a) CARLA data. (b) Sample rollouts overlaid, showing learned multimodality. (c) MFP learned semantically meaningful latent modes automatically: *triangle*: right turn, *square*: straight ahead, *circle*: stop.

4.1 CARLA

CARLA is a realistic, open-source, high fidelity driving simulator based on the Unreal Engine [17]. It currently contains six different towns and dozens of different vehicle assets. The simulation includes both highways and urban settings with traffic light intersections and four-way stops. Simple traffic law abiding "auto-pilot" CPU agents are also available.

We create a scenario at an intersection where one vehicle is approaching the intersection and two other vehicles are moving across horizontally (Fig. 4(a)). The first vehicle (red) has 3 different possibilities which are randomly chosen during data generation. The first mode aggressively speeds up and makes the right turn, cutting in front of the green vehicle. The second mode will still make the right turn, however it will slow down and yield to the green vehicle. For the third mode, the first vehicle will slow to a stop, yielding to both of the other vehicles. The far left vehicle also chooses randomly between going straight or turning right. We report the performance of MFP as a function of # of modes in Table 1.

Metric (nats)	C.V.	RNN basic	MFP 1 mode	MFP 2 modes	MFP 3 modes	MFP 4 modes	MFP 5 modes
NLL	11.46	5.64±0.02	5.23±0.01	3.37±0.81	1.72±0.19	1.39±0.01	1.39±0.01

Table 1: Test performance (minMSD with $K = 12$) comparisons.

NLL	Fixed-Encoding	DynEnc
	1.878±0.163	1.694±0.175
NLL	Teacher-forcing	Classmates-forcing
	4.344±0.059	4.196±0.075

Table 2: Additional comparisons.

Metric	Vehicle 1		Vehicle 2	
	Standard	Hypo	Standard	Hypo
K=12				
minADE	1.509 ± 0.37	1.402 ± 0.34	0.800 ± 0.064	0.709 ± 0.060
minFDE	2.530 ± 0.635	2.305 ± 0.570	3.171 ± 0.462	2.729 ± 0.415

Table 3: Hypothetical Rollouts.

The modes learned here are somewhat semantically meaningful. In Fig. 4(c), we can see that even for different vehicles, the same latent variable z learned to be interpretable. Mode 0 (squares) learned to go straight, mode 1 (circles) learned to break/stop, and mode 2 (triangles) represents right turns. Finally, in Table 2, we can see the performance between using teacher-forcing vs. the proposed classmates-forcing. In addition, we compare different types of encodings. DynEnc is the encoding proposed in Sec. 3.1. Fixed-encoding uses a fixed ordering which is not ideal when there are N arbitrary number of agents. We can also look at how well we can perform hypothetical rollouts by conditioning our predictions of other agents on ego's future trajectories. We report these results in Table 3.

	DESIRE [21]	SocialGAN	R2P2-MA [30]	ESP[30] no LIDAR	ESP	ESP Flex	MultiPath [8]	MFP-1	MFP-2	MFP-3	MFP-4	MFP-5
Town01	2.422	1.141	0.770	1.102	0.675	0.447	0.68	0.448	0.291	0.284	0.279	0.374
test	± 0.017	± 0.015	± 0.008	± 0.011	± 0.007	± 0.009		± 0.007	± 0.005	± 0.005	± 0.005	± 0.006
Town02	1.697	0.979	0.632	0.784	0.565	0.435	0.69	0.457	0.311	0.295	0.290	0.389
test	± 0.017	± 0.015	± 0.011	± 0.013	± 0.009	± 0.011		± 0.004	± 0.003	± 0.003	± 0.003	± 0.004

Table 4: Test performance (minMSD with $K = 12$) comparisons, in meters squared.

Metric	time	Cons vel.	CVGMM[15]	[23]	MATF[39]	LSTM	S-LSTM[1]	CS-LSTM(M)	MFP-1	MFP-2	MFP-3	MFP-4	MFP-5
NLL(nats)	1 sec.	3.72	2.02	-	-	1.17	1.01	0.89 (0.58)	0.73 \pm 0.01	-0.32 \pm 0.01	-0.58 \pm 0.01	-0.65\pm0.01	-0.45 \pm 0.01
	2 sec.	5.37	3.63	-	-	2.85	2.49	2.43 (2.14)	2.33 \pm 0.01	1.43 \pm 0.01	1.26 \pm 0.01	1.19\pm0.01	1.36 \pm 0.01
	3 sec.	6.40	4.62	-	-	3.80	3.36	3.30 (3.03)	3.17 \pm 0.01	2.45 \pm 0.01	2.32 \pm 0.01	2.28\pm0.01	2.42 \pm 0.01
	4 sec.	7.16	5.35	-	-	4.48	4.01	3.97 (3.68)	3.77 \pm 0.01	3.21 \pm 0.00	3.07 \pm 0.00	3.06\pm0.00	3.17 \pm 0.00
	5 sec.	7.76	5.93	-	-	4.99	4.54	4.51 (4.22)	4.26 \pm 0.00	3.81 \pm 0.00	3.69\pm0.00	3.69\pm0.00	3.76 \pm 0.00
Metric	time	Cons vel.	CVGMM		MATF	LSTM	S-LSTM	CS-LSTM[16]	MFP-1	MFP-2	MFP-3	MFP-4	MFP-5
RMSE(m)	1 sec.	0.73	0.66	0.69	0.66	0.68	0.65	0.61	0.54\pm0.00	0.55 \pm 0.00	0.54 \pm 0.00	0.54 \pm 0.00	0.55 \pm 0.00
	2 sec.	1.78	1.56	1.51	1.34	1.65	1.31	1.27	1.16\pm0.00	1.18 \pm 0.00	1.17 \pm 0.00	1.16 \pm 0.00	1.18 \pm 0.00
	3 sec.	3.13	2.75	2.55	2.08	2.91	2.16	2.09	1.90\pm0.00	1.92 \pm 0.00	1.91 \pm 0.00	1.89 \pm 0.00	1.92 \pm 0.00
	4 sec.	4.78	4.24	3.65	2.97	4.46	3.25	3.10	2.78\pm0.00	2.80 \pm 0.00	2.78 \pm 0.00	2.75 \pm 0.00	2.78 \pm 0.00
	5 sec.	6.68	5.99	4.71	4.13	6.27	4.55	4.37	3.83\pm0.01	3.85 \pm 0.01	3.83 \pm 0.01	3.78 \pm 0.01	3.80 \pm 0.01

Table 5: NGSIM prediction results. Hightlighted columns are our results (lower is better). MFP- K : K is the number of latent modes. The standard error of the mean is over 5 trials. For multimodal MFPs, we report minRMSE over 5 samples. NLL can be negative as we are modeling a continuous density function.

CARLA PRECOG

We next compared MFP to a much larger CARLA dataset with published benchmark results. This dataset consists of over 60K training sequences collected from two different towns in CARLA [30]. We trained MFP (with 1 to 5 modes) on the Town01 training set for 200K updates, with minibatch size 8. We report the minMSD metric (in meters squared) at $\hat{m}_{K=12}$ for all 5 agents *jointly*. We compare with state-of-the-art methods in Table 4. Non-MFP results are reported from [30] (v3) and [8]. MFP significantly outperforms various other methods on this dataset. We include qualitative visualizations of test set predictions in the supplementary materials.

4.2 NGSIM

Next Generation Simulation [12](NGSIM) is a collection of video-transcribed datasets of vehicle trajectories on US-101, Lankershim Blvd. in Los Angeles, I-80 in Emeryville, CA, and Peachtree St. in Atlanta, Georgia. In total, it contains approximately 45 minutes of vehicle trajectory data at 10 Hz and consisting of diverse interactions among cars, trucks, buses, and motorcycles in congested flow.

We experiment with the US-101 and I-80 datasets, and follow the experimental protocol of [16], where the datasets are split into 70% training, 10% validation, and 20% testing. We extract 8 seconds trajectories, using the first 3 seconds as history to predict 5 seconds into the future.

In Table 5, we report both neg. log-likelihood and RMSE errors on the test set. RMSE and other measures such as average/final displacement errors (ADE/FDE) are not good metrics for multimodal distributions and are only reported for MFP-1. For multimodal MFPs, we report minRMSE over 5 samples, which uses the ground truth select the best trajectory and therefore could be overly optimistic. Note that this applies equally to other popular metrics such as minADE, minFDE, and minMSD.

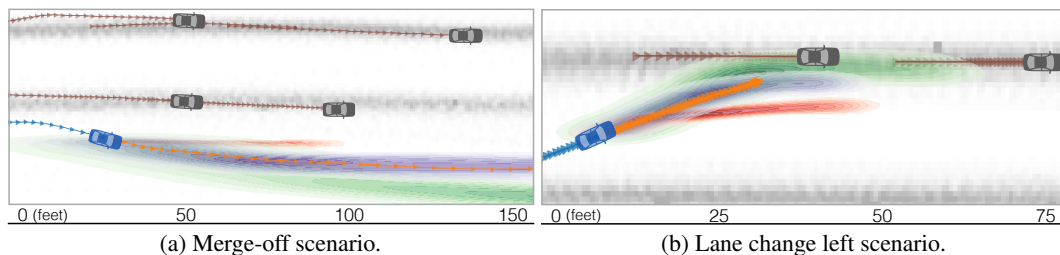


Figure 5: Qualitative MFP-3 results after training on NGSIM data. Three modes: red, purple, and green are shown as density contour plots for the blue vehicle. Grey vehicles are other agents. Blue path is past trajectory, orange path is actual future ground truth. Grey pixels form a heatmap of frequently visited paths. Additional visualizations provided in the supplementary materials.

The current state-of-the-art, multimodal CS-LSTM [16], requires a separate prediction of 6 fixed maneuver modes. As a comparison, MFP achieves significant improvements with less number of modes. Detailed evaluation protocols are provided in the supplementary materials. We also provide qualitative results on the different modes learned by MFP in Fig. 5. In the right panel, we can interpret the green mode is fairly aggressive lane change while the purple and red mode is more “cautious”. Ablative studies showing the contributions of both interactive rollouts and dynamic attention encoding are also provided in the supplementary materials. We obtain best performance with the combination of both interactive rollouts and dynamic attention encoding.

4.3 Argoverse Motion Forecasting

Argoverse motion forecasting dataset is a large scale trajectory prediction dataset with more than 300,000 curated scenarios [9]. Each sequence is 5 seconds long in total and the task is to predict the next 3 seconds after observing 2 seconds of history. We performed preliminary experiments by training a MFP with 3 modes for 20K updates and compared to the existing official baselines in Table 6. MFP hyperparameters were not selected for this dataset so we do expect to see improved MFP performances with additional tuning. We report validation set performance on both version 1.0 and version 1.1 of the dataset.

minADE	C.V.	NN+map	LSTM+ED	LSTM	MFP3	MFP3
K=6				ED+map	(ver. 1.0)	(ver. 1.1)
meters	3.55	2.28	2.27	2.25	1.411	1.399

Table 6: Argoverse Motion Forecasting. Performance on the validation set. CV: constant velocity. Baseline results are from [9].

4.4 Planning and Decision Making

The original intuitive motivation for learning a good predictor is to enable robust decision making. We now test this by creating a simple yet non-trivial reinforcement learning (RL) task in the form of an unprotected left turn. Situated in Town05 of the CARLA simulator, the objective is to safely perform an unprotected (no traffic lights) turn, see Fig. 6. Two oncoming vehicles have random initial speeds. Collisions incur a penalty of -500 while success yields $+10$. There is also a small reward for higher velocity and the action space is acceleration along the ego agent’s default path (blue).

Using predictions to learn the policy is in the domain of model-based RL [33, 37]. Here, MFP can be used in several ways: 1) we can generate imagined future rollouts and add them to the experiences from which temporal difference methods learns [33], or 2) we can perform online planning by using a form of the shooting methods [5], which allows us to optimize over future trajectories. We perform experiments with the latter technique where we progressively train MFP to predict the joint future trajectories of all three vehicles in the scene. We find the optimal policy by leveraging the current MFP model and optimize over ego’s future actions. We compare this approach to a couple of strong model-free RL baselines: DDPG and Proximal policy gradients. In Fig. 7, we plot the reward vs. the number of environmental steps taken. In Table 7, we show that MFP based planning is more robust to parameter variations in the testing environment.



Figure 6: RL learning environment - Unprotected left turn.

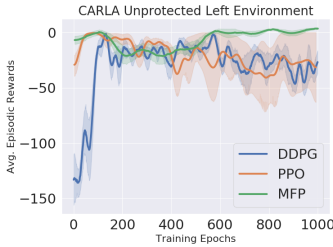


Figure 7: Learning curves as a function of step sizes.

Δ Env. Params	DDPG	PPO	MFP
vel : $+0m/s$	3%	4%	0%
vel : $+5m/s$	8%	4%	0%
vel : $+10m/s$	6%	15%	0%
acc : $+1m/s^2$	3%	1%	0%

Table 7: Testing crash rates per 100 trials. Test env. modifies the velocity & acceleration parameters.

5 Discussions

In this paper, we proposed a probabilistic latent variable framework that facilitates the joint multi-step temporal prediction of arbitrary number of agents in a scene. Leveraging the ability to learn latent modes directly from data and interactively rolling out the future with different point-of-view encoding, MFP demonstrated *state-of-the-art* performance on several vehicle trajectory datasets. For future work, it would be interesting to add a mix of discrete and continuous latent variables as well as train and validate on pedestrian or bicycle trajectory datasets.

Acknowledgements We thank Barry Theobald, Russ Webb, Nitish Srivastava, and the anonymous reviewers for making this a better manuscript. We also thank the authors of [16] for open sourcing their code and dataset.

References

- [1] Alexandre Alahi, Kratarth Goel, Vignesh Ramanathan, Alexandre Robicquet, Li Fei-Fei, and Silvio Savarese. Social lstm: Human trajectory prediction in crowded spaces. In *Proceedings of the IEEE conference on computer vision and pattern recognition*, pages 961–971, 2016.
- [2] Mayank Bansal, Alex Krizhevsky, and Abhijit S. Ogale. Chauffeurnet: Learning to drive by imitating the best and synthesizing the worst. *CoRR*, abs/1812.03079, 2018.
- [3] Justin Bayer and Christian Osendorfer. Learning stochastic recurrent networks. *arXiv preprint arXiv:1411.7610*, 2014.
- [4] Samy Bengio, Oriol Vinyals, Navdeep Jaitly, and Noam Shazeer. Scheduled sampling for sequence prediction with recurrent neural networks. In *Advances in Neural Information Processing Systems*, pages 1171–1179, 2015.
- [5] John T Betts. Survey of numerical methods for trajectory optimization. *Journal of guidance, control, and dynamics*, 21(2):193–207, 1998.
- [6] Yuri Burda, Roger Grosse, and Ruslan Salakhutdinov. Importance weighted autoencoders. *arXiv preprint arXiv:1509.00519*, 2015.
- [7] Sergio Casas, Wenjie Luo, and Raquel Urtasun. Intentnet: Learning to predict intention from raw sensor data. In Aude Billard, Anca Dragan, Jan Peters, and Jun Morimoto, editors, *Proceedings of The 2nd Conference on Robot Learning*, volume 87 of *Proceedings of Machine Learning Research*, pages 947–956. PMLR, 29–31 Oct 2018.
- [8] Yuning Chai, Benjamin Sapp, Mayank Bansal, and Dragomir Anguelov. Multipath: Multiple probabilistic anchor trajectory hypotheses for behavior prediction. *arXiv preprint arXiv:1910.05449*, 2019.
- [9] Ming-Fang Chang, John Lambert, Patsorn Sangkloy, Jagjeet Singh, Slawomir Bak, Andrew Hartnett, De Wang, Peter Carr, Simon Lucey, Deva Ramanan, et al. Argoverse: 3d tracking and forecasting with rich maps. In *Proceedings of the IEEE Conference on Computer Vision and Pattern Recognition*, pages 8748–8757, 2019.
- [10] Junyoung Chung, Caglar Gulcehre, KyungHyun Cho, and Yoshua Bengio. Empirical evaluation of gated recurrent neural networks on sequence modeling. *arXiv preprint arXiv:1412.3555*, 2014.
- [11] Junyoung Chung, Kyle Kastner, Laurent Dinh, Kratarth Goel, Aaron C Courville, and Yoshua Bengio. A recurrent latent variable model for sequential data. In *Advances in neural information processing systems*, pages 2980–2988, 2015.
- [12] James Colyar and John Halkias. Us highway 101 dataset. FHWA-HRT-07-030, 2007.
- [13] Henggang Cui, Vladan Radosavljevic, Fang-Chieh Chou, Tsung-Han Lin, Thi Nguyen, Tzu-Kuo Huang, Jeff Schneider, and Nemanja Djuric. Multimodal trajectory predictions for autonomous driving using deep convolutional networks. *CoRR*, abs/1809.10732, 2018.
- [14] A. P. Dempster, N. M. Laird, and D. B. Rubin. Maximum likelihood from incomplete data via the EM algorithm. *Journal of the Royal Statistical Society: Series B*, 39:1–38, 1977.
- [15] Nachiket Deo, Akshay Rangesh, and Mohan M Trivedi. How would surround vehicles move? a unified framework for maneuver classification and motion prediction. *IEEE Transactions on Intelligent Vehicles*, 3(2):129–140, 2018.
- [16] Nachiket Deo and Mohan M. Trivedi. Convolutional social pooling for vehicle trajectory prediction. *CoRR*, abs/1805.06771, 2018.
- [17] Alexey Dosovitskiy, German Ros, Felipe Codevilla, Antonio Lopez, and Vladlen Koltun. CARLA: An open urban driving simulator. In *Proceedings of the 1st Annual Conference on Robot Learning*, pages 1–16, 2017.
- [18] Marco Fraccaro, Søren Kaae Sønderby, Ulrich Paquet, and Ole Winther. Sequential neural models with stochastic layers. In *Advances in neural information processing systems*, pages 2199–2207, 2016.
- [19] Anirudh Goyal, Alessandro Sordani, Marc-Alexandre Côté, Nan Rosemary Ke, and Yoshua Bengio. Z-forcing: Training stochastic recurrent networks. In *Advances in neural information processing systems*, pages 6713–6723, 2017.
- [20] Karol Gregor, Ivo Danihelka, Alex Graves, Danilo Jimenez Rezende, and Daan Wierstra. Draw: A recurrent neural network for image generation. *arXiv preprint arXiv:1502.04623*, 2015.
- [21] Tuomas Haarnoja, Anurag Ajay, Sergey Levine, and Pieter Abbeel. Backprop KF: learning discriminative deterministic state estimators. *CoRR*, abs/1605.07148, 2016.

- [22] Thomas Howard, Mihail Pivtoraiko, Ross A Knepper, and Alonzo Kelly. Model-predictive motion planning: Several key developments for autonomous mobile robots. *IEEE Robotics & Automation Magazine*, 21(1):64–73, 2014.
- [23] Alex Kuefler, Jeremy Morton, Tim Wheeler, and Mykel Kochenderfer. Imitating driver behavior with generative adversarial networks. In *2017 IEEE Intelligent Vehicles Symposium (IV)*, pages 204–211. IEEE, 2017.
- [24] Namhoon Lee, Wongun Choi, Paul Vernaza, Chris Choy, Philip H. S. Torr, and Manmohan Chandraker. Desire: Distant future prediction in dynamic scenes with interacting agents. pages 2165–2174, 07 2017.
- [25] Stéphanie Lefèvre, Dizan Vasquez, and Christian Laugier. A survey on motion prediction and risk assessment for intelligent vehicles. *ROBOMECH journal*, 1(1):1, 2014.
- [26] Yuexin Ma, Xinge Zhu, Sibozhang, Ruigang Yang, Wenping Wang, and Dinesh Manocha. Trafficpredict: Trajectory prediction for heterogeneous traffic-agents. *CoRR*, abs/1811.02146, 2018.
- [27] Radford M Neal and Geoffrey E Hinton. A view of the em algorithm that justifies incremental, sparse, and other variants. In *Learning in graphical models*, pages 355–368. Springer, 1998.
- [28] Brian Paden, Michal Cap, Sze Zheng Yong, Dmitry Yershov, and Emilio Frazzoli. A survey of motion planning and control techniques for self-driving urban vehicles. *IEEE Transactions on Intelligent Vehicles*, 1, 04 2016.
- [29] SeongHyeon Park, Byeongdo Kim, Chang Mook Kang, Chung Choo Chung, and Jun Won Choi. Sequence-to-sequence prediction of vehicle trajectory via LSTM encoder-decoder architecture. *CoRR*, abs/1802.06338, 2018.
- [30] Nicholas Rhinehart, Rowan McAllister, Kris M. Kitani, and Sergey Levine. PRECOG: prediction conditioned on goals in visual multi-agent settings. *CoRR*, abs/1905.01296, 2019.
- [31] Chen Sun, Per Karlsson, Jiajun Wu, Joshua B. Tenenbaum, and Kevin Murphy. Stochastic prediction of multi-agent interactions from partial observations. *CoRR*, abs/1902.09641, 2019.
- [32] Ilya Sutskever, Oriol Vinyals, and Quoc V Le. Sequence to sequence learning with neural networks. In *Advances in neural information processing systems*, pages 3104–3112, 2014.
- [33] Richard S Sutton. Integrated architectures for learning, planning, and reacting based on approximating dynamic programming. In *Machine Learning Proceedings 1990*, pages 216–224. Elsevier, 1990.
- [34] Sebastian Thrun, Mike Montemerlo, Hendrik Dahlkamp, David Stavens, Andrei Aron, James Diebel, Philip Fong, John Gale, Morgan Halpenny, Gabriel Hoffmann, et al. Stanley: The robot that won the darpa grand challenge. *Journal of field Robotics*, 23(9):661–692, 2006.
- [35] Ashish Vaswani, Noam Shazeer, Niki Parmar, Jakob Uszkoreit, Llion Jones, Aidan N Gomez, Łukasz Kaiser, and Illia Polosukhin. Attention is all you need. In *Advances in neural information processing systems*, pages 5998–6008, 2017.
- [36] Nicholas Watters, Daniel Zoran, Theophane Weber, Peter Battaglia, Razvan Pascanu, and Andrea Tacchetti. Visual interaction networks: Learning a physics simulator from video. In *Advances in neural information processing systems*, pages 4539–4547, 2017.
- [37] Theophane Weber, Sébastien Racanière, David P. Reichert, Lars Buesing, Arthur Guez, Danilo Jimenez Rezende, Adrià Puigdomènech Badia, Oriol Vinyals, Nicolas Heess, Yujia Li, Razvan Pascanu, Peter W. Battaglia, David Silver, and Daan Wierstra. Imagination-augmented agents for deep reinforcement learning. *CoRR*, abs/1707.06203, 2017.
- [38] Greg Welch, Gary Bishop, et al. An introduction to the kalman filter. 1995.
- [39] Tianyang Zhao, Yifei Xu, Mathew Monfort, Wongun Choi, Chris Baker, Yibiao Zhao, Yizhou Wang, and Ying Nian Wu. Multi-agent tensor fusion for contextual trajectory prediction. *CoRR*, abs/1904.04776, 2019.

Supplementary Materials

6 MFP Implementation Details

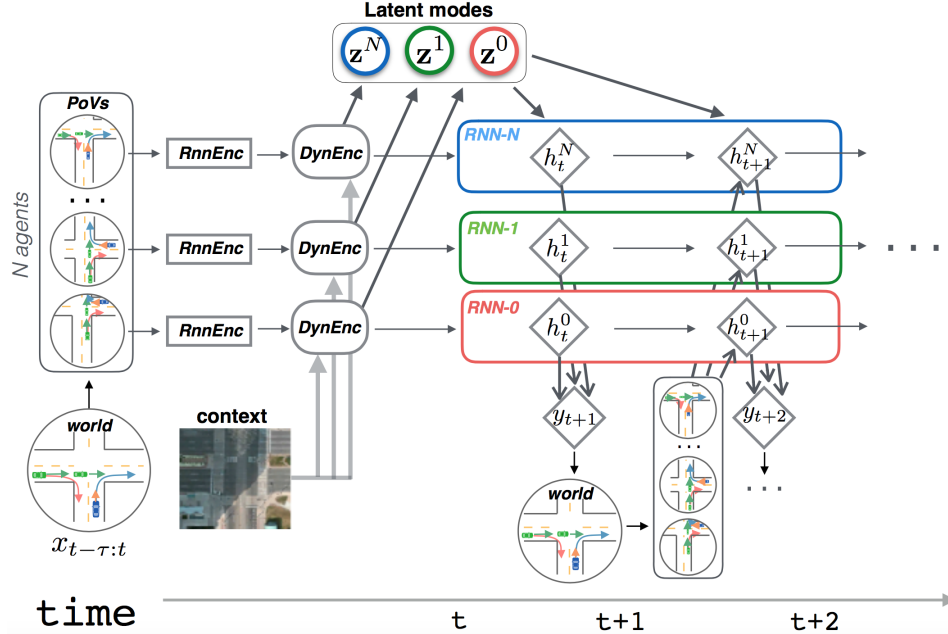


Figure 8: MFP Architecture.

6.1 Architecture

For all of our experiments we use the same model architecture for the MFP. The input observations consist of 2 dimensional x, y , positions of the agent. Both encoders and decoders are using bidirectional GRUs. The encoder RNNs have a hidden dimension of 64 while the decoder RNNs have a hidden layer size of 128. For nonlinear activation functions we use the rectified linear (ReLU) activations.

Context: Context information is encoded by two layers of standard 3×3 convolutional layers followed by one 2d max-pooling layer, followed by one more 3×3 convolutional and finally a fully connected layer with an output dimensionality of 64.

Dynamic encoding: For dynamic encoding we use a small neural network of 32 units each to transform every agent state (position) into an 8 dimensional key. The encoder has 8 slots, where each slot has a learnable key. Matching is performed using Radial Basis function $RBF(k, k') = \exp(-\frac{\|k-k'\|_2^2}{T})$, where T is the temperature and set to 1.0. Match scores are used as part of a soft-attention mechanism to weight the contribution of each encoder RNN features and aggregated into the 8 slots. The input vector of the 8 slots are transformed by a 3 hidden layer network into a feature encoding of size 32.

Latent modes: A single linear layer is used to project the concatenated feature encodings into a Softmax which represent the distribution over the K modes. The input dimension consists of $64 + 32 + 32 = 128$ dimensions and the output dimensions is K .

Decoder: The decoder RNNs consist of bi-directional GRUs with 128 dimensional hidden layers and are initialized with the contextual features at timestep t .

Normalization: We found that training is accelerated by computing the average future trajectory positions (constant across samples) and subtracting it off from the future prediction targets. In addition, we normalize the past historical trajectories by subtracting off the position of the agents at time t , such that the position of each agent at time t for its own RNN would be $(0.0, 0.0)$.

6.2 Algorithm

We provide the pseudo-code to MFP training in the Algorithm 1.

Algorithm 1: MFP training algorithm

Input : Dataset $\mathcal{D} = \{(\mathbf{X}^{(i)}, \mathbf{Y}^{(i)}) \dots\}_{i=1,2,\dots,|\mathcal{D}|}$, # of modes M
Initialize : Randomly initialize MFP network, encoders, decoders, and all parameters.

```
1 for iterations  $i = 0$  to  $T$  do
2   Randomly sample a neighborhood trajectory cluster from  $\mathcal{D}$ .
3   Normalization of trajectories.
   // forward pass
4   for agent  $i$  in cluster do
   |    $\mathbf{h}_i \leftarrow$  GRU encoder of past history of agent  $i$ 
   end
5    $\mathcal{I} \leftarrow$  Contextual encoding of the scene.
6   Dynamic Attention Encoding (Sec. 3.1):  $\mathbf{f} \leftarrow DynEnc(\{\mathbf{h}_i\}, \mathcal{I})$ .
7   for modes  $m = 1$  to  $M$  do
8     for steps  $\delta = t + 1$  to  $T$  do
9       for agent  $i$  in cluster do
10        Set  $z^i$  according to mode  $m$  (one-hot encoding).
11         $\mathbf{e}_i \leftarrow DynEnc(\varphi(\hat{\mathbf{Y}}_{\delta-1}))$  // DynEnc of past state of all agents with agent
12         $i$ 's point-of-view
13        For classmates-forcing use ground truth  $\mathbf{y}_{\delta-1}^n$  when  $n \neq i$ .
14         $\hat{\mathbf{y}}_{\delta}^i \leftarrow RnnDecode(\mathbf{e}_i, z^i, \mathbf{f})$ 
15      end
16      Update predicted  $\hat{\mathbf{Y}}_{\delta} = \{\hat{\mathbf{y}}_{\delta}^i\}_{i=0:N}$ 
17    end
18  end
19  Compute loss.
20  /* E-step
21  Compute true posterior  $p(\mathbf{Z}|\mathbf{Y}, \mathbf{X}; \theta)$ 
22  /* M-step
23  Backpropagation through time over entire forward computation graph (weighted by the posterior).
24  Update approximating prior:  $\partial KL(p(\mathbf{Z}|\mathbf{Y}, \mathbf{X}; \theta') || p(\mathbf{Z}|\mathbf{X}; \theta_Z)) / \partial \theta_Z$ 
25 end
```

Table 8: Comparison to existing work on vehicle trajectory predictions.

Methods	Multimodal	No-labeling of Modes	Variational	Inter. Rollouts	Inter. Encodings	Context	Hypothetical
CS-LSTM	✓	×	×	×	✓	×	×
Seq2Seq	×	-	×	×	✓	×	×
TrafficPredict	×	-	×	✓	✓	×	×
Cui et al. (Uber)	✓	✓	×	×	✓	✓	×
DESIRE	✓	✓	✓	×	✓	✓	×
IntentNet	✓	×	×	×	✓	✓	×
ChaufferNet	×	-	×	×	✓	✓	×
MFP (Ours)	✓	✓	✓	✓	✓	✓	✓

6.3 Feature Comparisons

We provide a comparison of our proposed MFP and some of the existing prior work on trajectory predictions in the table below. “Variational” approaches maximize a variational lower-bound during optimization. “Interactive rollouts” means that the future predicted states of one agent will interact with the future predictions of other agents. “Hypothetical” refers to whether a model is able to change its prediction depending on a hypothetical ego future trajectory.

7 Carla Experiments

For CARLA experiments, we collected trajectory data for 3 vehicles in an intersection from the map *Town-05*. We generate data at 20 Hz by simulating forward for 5 seconds. The position of vehicles are initialized at the same location with a Gaussian noise of ± 0.2 meters. The red vehicle in Fig. 4(a) has 3 different modes: *right turn fast*, *right turn slow*, *stop/yield*, which are selected at random. The far-left blue vehicle can also go straight or turn right, chosen randomly. We generate 100 trajectories from random simulations in total.

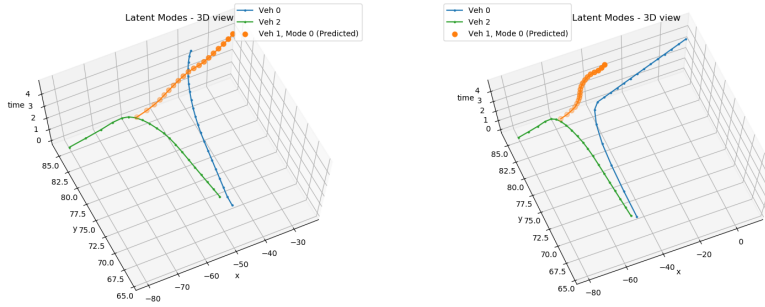


Figure 9: The same mode results in different behaviors due to interactions. Orange trajectory for left and right rollouts are from the same mode. However, as the blue trajectory changes, the interaction affects the rollout of the orange trajectory (vehicle 1).

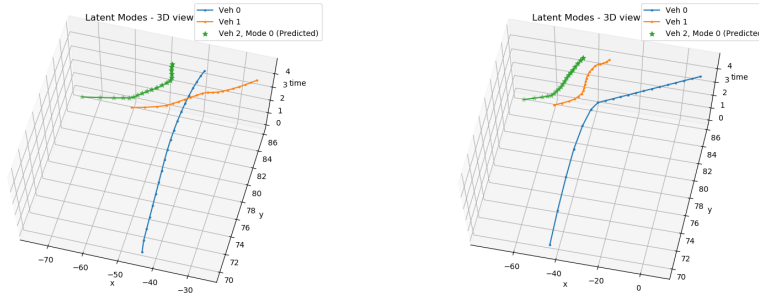


Figure 10: The same mode results in different behaviors due to interactions. Green and orange trajectory for left and right rollouts are from the same mode. However, as the blue trajectory changes, the interaction affects the rollout of both vehicles 1 and 2.

7.1 Interactions

One interesting properties of the interactive future rollout of the MFP is that interaction allows the same mode to take on multiple trajectories. As an example, vehicle 1 might be in an aggressive mode, but depending on whether or not another vehicle cut in front of vehicle 1, it will never-the-less have a different trajectory. This means that having interactions in *future* joint rollouts allows MFP to model more variation with less latent modes. We illustrate this with a couple of examples in Fig. 9 and Fig. 10.

7.2 Carla PRECOG

We qualitatively visualize prediction results of MFP-4 on the test sets of Town01 and Town02 in Figs. 11 and 12. We overlay predictions on top of Lidar point clouds. Predictions are very accurate and the trajectories do not seem to contain more than two modes, as can also be seen in the quantitative experiments. In this case, MFP’s attention-based state encoding becomes critical to learning accurate predictions. We also note that the quantitative minMSD results have improved significantly from the previous version of this paper. The main differences are due to the increase of the size of the minibatch from 1 to 8 during training and better data normalization.

8 NGSIM Experiments

For NGSIM experiments, we used 6 sequences from the US-101 and I-80 datasets and randomly split them into 70% training, 10% validation, and 20% testing, resulting in 5922867 samples for training, 859769 samples for validation, and 1505756 samples for testing. Following practice of existing work, we use 3 seconds for past history while predicting the next 5 seconds into the future. We perform subsampling by a factor of 2 so every timestep is 200 ms.

Results from Table 6 are over 5 random trials where we report the standard error of the mean. For all MFP models we reported errors using the saved model parameters after 300K parameter updates.

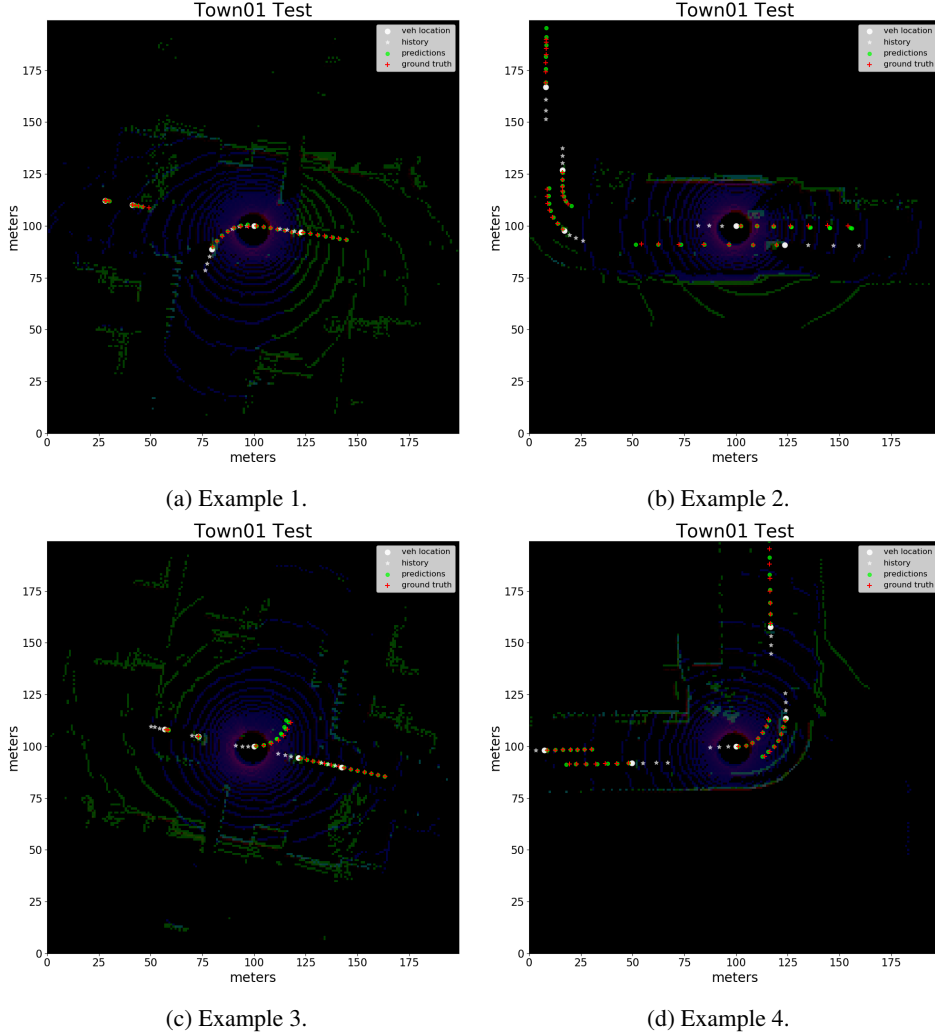


Figure 11: Qualitative joint predictions from Town01 test set.

The dataset is openly available here: <https://data.transportation.gov/Automobiles/Next-Generation-Simulation-NGSIM-Vehicle-Trajectory/8ect-6jqj>.

8.1 Training

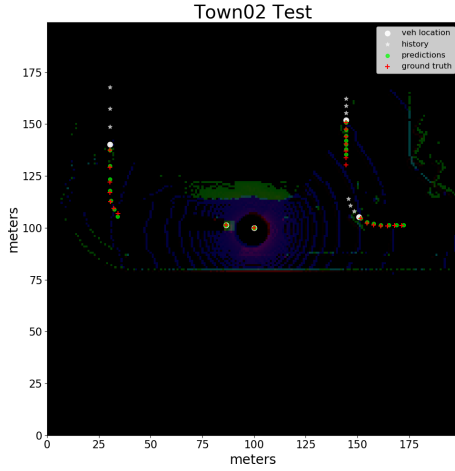
For training, we use the ADAM optimizer with stochastic minibatches of trajectory samples. For the NGSIM experiments, the minibatch size varies depending on the density of vehicles around a particular region. The average minibatch size is 60, but minibatch size of 1 or ≥ 200 are also possible. The initial learning rate is set at 0.001 and are decreased by a factor of 10 every 100K updates. We lower-bound the learning rate to be 0.00005. In order to accelerate training, we first pretrain MFP without interactive rollouts for 200K updates before continuing to train with interactive rollouts for an additional 100K parameter updates.

8.2 Runtime

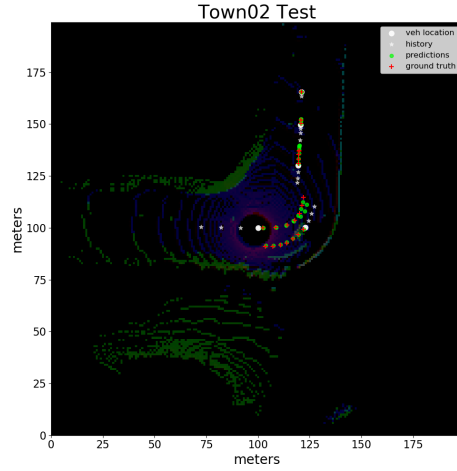
For NGSIM experiments, a training run is performed using a single nVidia Titan X GPU using the pyTorch 1.0.1 framework. During training, each batch update takes roughly 1.2 seconds wall clock time. Each training run converges in approximately one day.

8.3 Ablative Studies

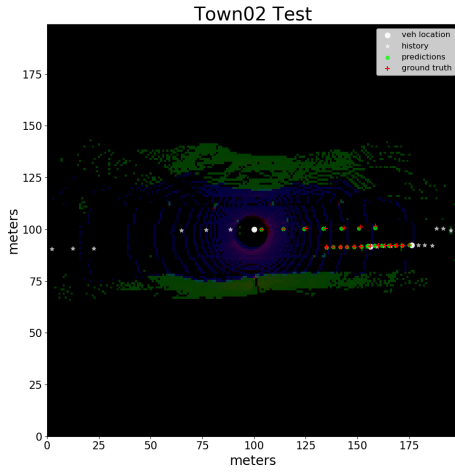
In Figure 14 we show the effects of interactions and dynamic encoding in NGSIM test performance. Best results are obtained with the utilization of both.



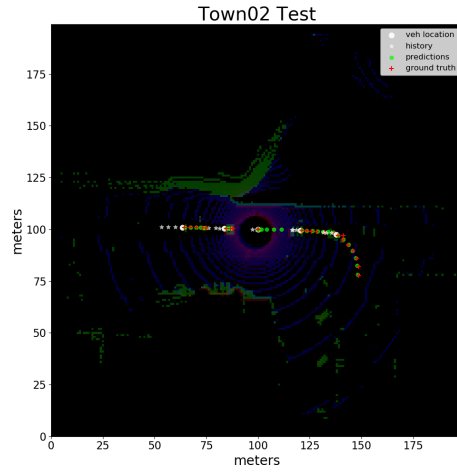
(a) Example 1.



(b) Example 2.



(c) Example 3.



(d) Example 4.

Figure 12: Qualitative joint predictions from Town02 test set.



Figure 13: NGSIM dataset.

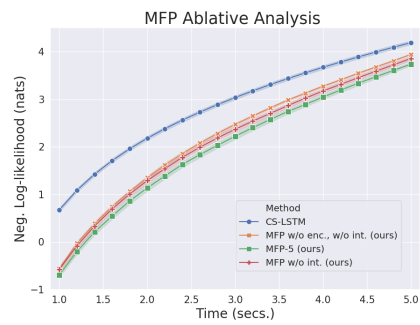
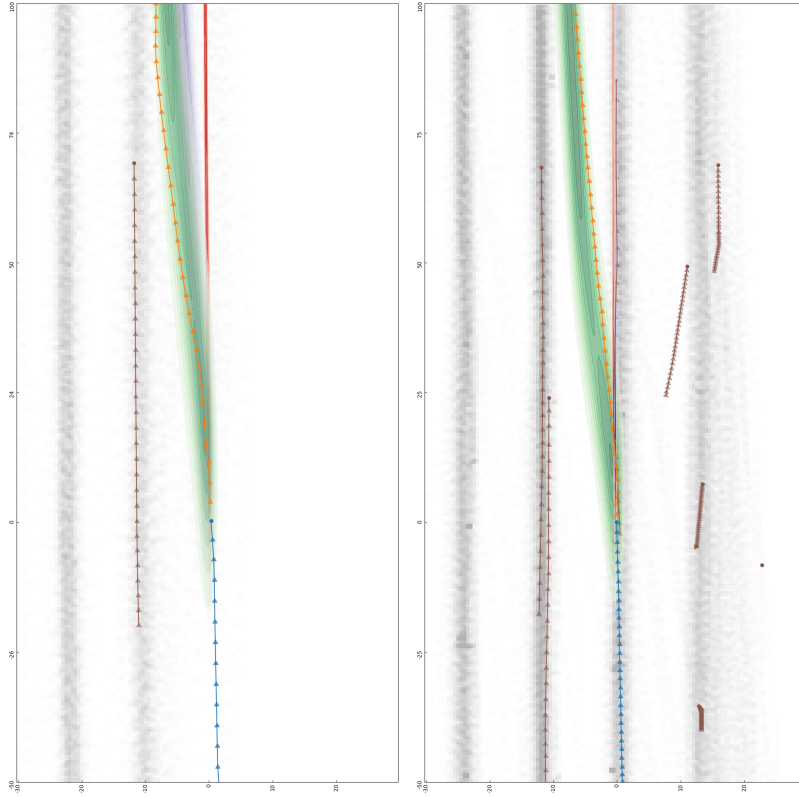


Figure 14: MFP ablative studies.

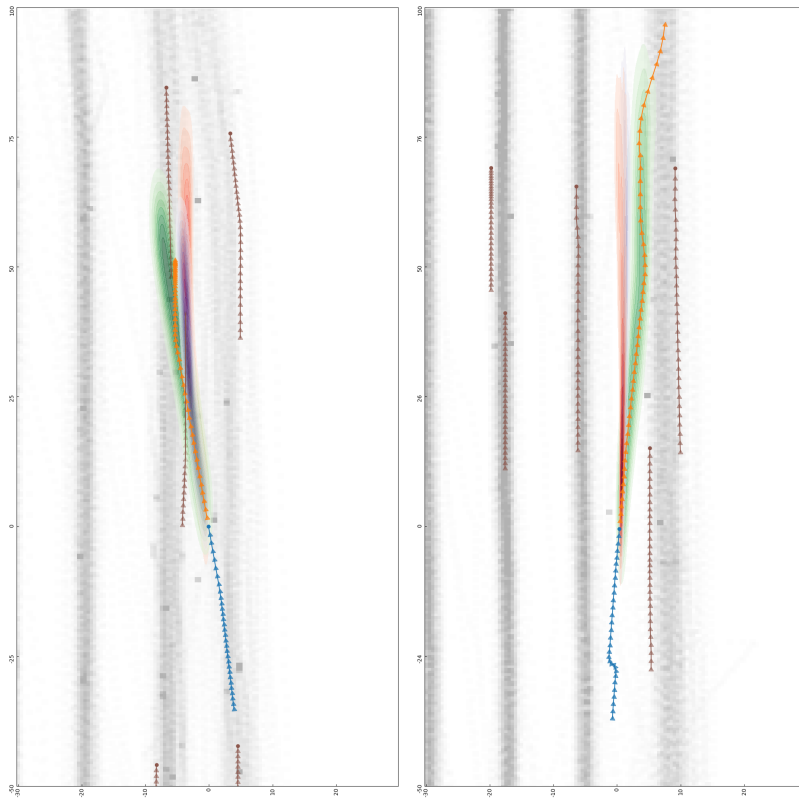
8.3.1 Additional Qualitative Experiments

We show additional qualitative experiments similar to the ones shown in Figure 5. The colors represent the three modes learned by MFP-3: red, purple, and green. Blue and brown paths are previous trajectories while the orange path is the future trajectory.



(a) Example 1.

(b) Example 2.



(c) Example 3.

(d) Example 4.

Figure 15: Additional qualitative plots showing MFP-3 modes learned from NGSIM dataset.